ISSN 1054-660X, Laser Physics, 2007, Vol. 17, No. 5, pp. 672–679.

Nonlinear Optics with Quantum Cascade Lasers

F. Xie[a], V. R. Chaganti[a], D. Smith[a], A. Belyanin[a,*], F. Capasso[b], and C. Gmachl[c]

[a] *Department of Physics, Texas A&M University, College Station, TX 77843-4242, USA*
[b] *Division of Engineering and Applied Sciences, Harvard University, Cambridge, MA 02138, USA*
[c] *Department of Electrical Engineering and PRISM, Princeton University, Princeton, NJ 08544, USA*
*e-mail: belyanin@tamu.edu

Received November 9, 2006

Abstract—We discuss new approaches to monolithic integration of quantum cascade lasers with resonant intersubband nonlinearities. We show that the proposed approaches can greatly enhance the performance of quantum cascade lasers and give rise to new functionalities. Examples considered include extreme frequency up- or down-conversion and wide-range electric tuning.

PACS numbers: 42.55.Px, 42.60.-k, 78.67.De, 85.35.Be

DOI: 10.1134/S1054660X07050118

1. INTRODUCTION

It was recently shown [1–10] that the active region of a quantum cascade (QC) laser can be integrated with a cascade of intersubband transitions designed for the nonlinear conversion of laser light into coherent radiation at different frequencies. In other words, the laser field serves as an intracavity optical pump or drive for the desired nonlinear optical interaction. Any intracavity optical pump loss (due either to resonant absorption or nonlinear optical processes) can be compensated by laser gain in the active nonlinear medium. This approach allows one to utilize the giant resonant optical nonlinearities associated with intersubband transitions in coupled quantum wells (QWs) [11–14]. From the practical point of view, it is important that monolithic integration yields compact, injection-pumped devices.

The monolithic approach to integrating nonlinear elements with QC lasers has been successful in experimentally demonstrating a wide range of nonlinear optical phenomena. Second harmonic generation (SHG), third harmonic generation, and sum-frequency generation (SFG) have all been reported. Refinements and optimizations to the original device designs have been made. Some classes of the optimized devices now have output suitable for practical application: Milliwatt power levels have been achieved for second harmonic generation [6]. Recently, the first successful Raman injection laser with 16 mW Stokes power and 30% conversion efficiency was reported [7].

In spite of the initial success and rapid optimization of monolithically integrated devices, all the devices demonstrated so far had certain shortcomings. Most importantly, monolithic devices did not show broad spectral tunability inherent to the nonlinear optical schemes with external nonlinear elements. Their tuning range was the same as for standard QC lasers. The reason for the limited flexibility was that the nonlinear mixing region shared the same intersubband transition structure and the same injection current with the QC laser active region. In this case, voltage and current across the device was essentially determined by laser operation; in particular, the voltage was pinned after reaching the laser threshold. This strongly limited ways to control the nonlinear optical process in the integrated nonlinear region.

Here, we discuss the design strategies that would create more possibilities for controlling the nonlinear processes and as a result, would allow one to enhance the tuning and wavelength range available for integrated devices. We find that the necessary condition for improved tunability, wavelength agility, and overall performance of the nonlinear devices is the independent control of the electric field in the nonlinear region, which can be achieved by adding a third terminal to the device. There are two basic ways to achieve that goal. In the first approach, the integration can be implemented in the growth direction by vertically stacking the nonlinear region and active laser stages. Then, a side contact controlling the voltage through the nonlinear region can be fabricated as shown in Fig. 1a. This approach allows completely independent design of the QC laser and nonlinear structures. However, it may lead to thicker epitaxial growth, complicated compound waveguide design, and current spreading due to side contacts.

The second method is the in-plane integration strategy in which we longitudinally divide the laser into separately contacted and biased sections along the laser cavity (Fig. 1b). All sections share the same epitaxial layer structure, but the electron states in each section depend on the applied bias. Thus, each section can be independently operated as either an active laser medium or a nonlinear element.

At the first glance, it may seem that in-plane integration should have a very limited range of applications, or

should not work at all. Indeed, one may expect it to be a lucky coincidence that the same structure can serve as a laser and as a nonlinear cascade *resonantly* pumped by this laser at two different biases. However, it turns out that such schemes can be surprisingly flexible in implementing various optical nonlinearities.

The generic in-plane integration scheme is shown in Fig. 1b. Independent of the details of the nonlinear interaction, there is one general requirement: The absorption of a nonlinear section should not kill the active laser. This implies that the gain in the laser section gL_1 should be higher than the sum of absorption losses in the nonlinear section $\alpha_{nl}L_2$ and all other losses. Typically, the optimal value of the product $\alpha_{nl}L_2$ is of the order of 1.

Below, we consider specific designs in which the nonlinear section serves as a Raman active region or a cascade for second harmonic generation. We show that this approach enables convenient tuning by applied voltage and allows one to extend the operation of QC lasers into very short or very long wavelengths.

2. BROADLY TUNABLE RAMAN LASER

Conventional QC lasers are based on resonant tunneling through a stack of coupled QWs and superlattices. They "resist" any tuning by the Stark effect above the laser threshold, after the alignment between the injector and the upper laser state is reached and population inversion gets pinned down to a threshold value. As a result, QC lasers can only be tuned over a limited range of a few cm^{-1} by changing the temperature of the heat sink or the injection current. In practice, a wide tuning range in QC laser-based sensors is achieved by using an external cavity system. Such systems require external optical elements and moving mechanical parts, which may be inconvenient.

Integration of QC lasers with resonant optical nonlinearities provides a new opportunity for fast and broad tuning by changing the bias voltage applied across the nonlinear optical element. For specificity, let us first examine this tuning mechanism for a vertically integrated Raman laser, with the Raman active region qualitatively similar to the one experimentally realized in [7] (see Fig. 2).

The possibility of Raman amplification using intersubband transitions has been theoretically discussed in [15]. In [16], Raman lasing on intersubband transition in a GaAs/AlGaAs double quantum well structure optically pumped by CO_2 laser has been demonstrated, although the Raman shift was still determined by phonon resonance. In [7], the first *injection-pumped* Raman laser was demonstrated, where the fundamental and the Raman radiations are both generated by intersubband electronic transitions in the very same active region of a quantum cascade laser (QCL). The stimulated scattering and lasing is due to the excitation of coherent electronic polarization on the mid-infrared

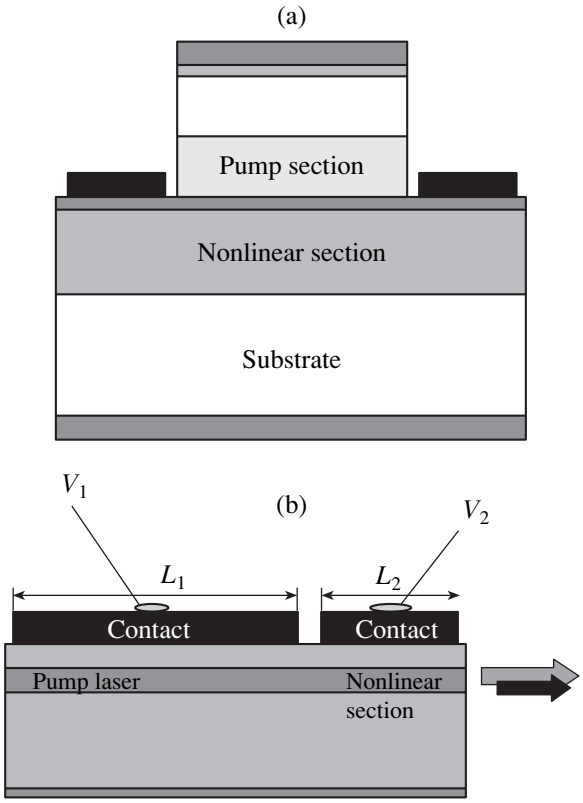

Fig. 1. (a) Cross section of a device with monolithic (vertical) integration of the pump laser and the nonlinear section, and side contacts (facet view); (b) in-plane integration of a QC laser pump with the nonlinear section (side view). Both schemes provide independent voltage control across the laser pump and nonlinear sections.

intersubband transition 2–1. Its frequency $(E_2 - E_1)/\hbar$ defines the Raman shift; it has nothing to do with phonons and can vary in a very broad range. It could also be efficiently tuned by a voltage bias, since the transition 2–1 is diagonal in real space.

One period of the Raman laser structure reported in [7] is shown in Fig. 2a. Laser light at 6.7 μm generated on the transition 6–5 serves as a resonant optical pump for lasing at the Stokes wavelength of 9 μm, which is detuned by 15 meV from the transition 3–2. Resonant absorption of the pump at the transition 1–3 is overcome by amplification in the pump laser section at the transition 6–5. The triply resonant nature of the process makes Raman scattering very efficient: peak fundamental power is only 40 mW at the threshold for Raman lasing, which implies a very large gain coefficient of the order of 2×10^{-5} cm/W per period (6×10^{-4} cm/W for the whole stack of 30 stages) and high efficiency of the nonlinear interaction. The nonlinear conversion efficiency around 30% has been measured. However, the tuning range of the Stokes radiation has been limited,

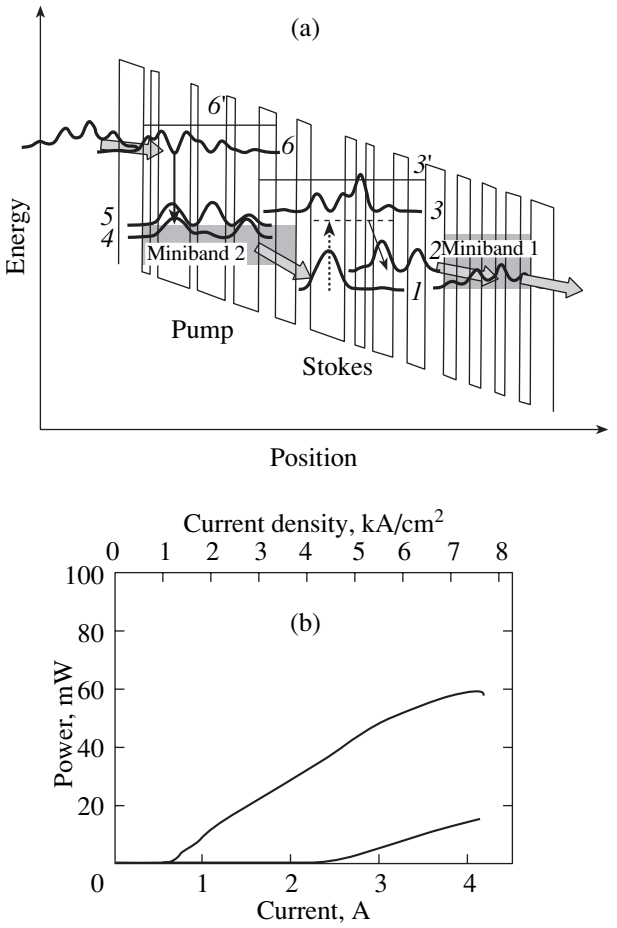

Fig. 2. (From [7].) (a) Active region of a resonant Raman laser that integrates fundamental laser cascade 6–5–4 and resonant Λ scheme of transitions 1–3–2–1 for Raman–Stokes lasing. (b) Laser (upper curve) and Stokes (lower curve) powers as functions of the injection current.

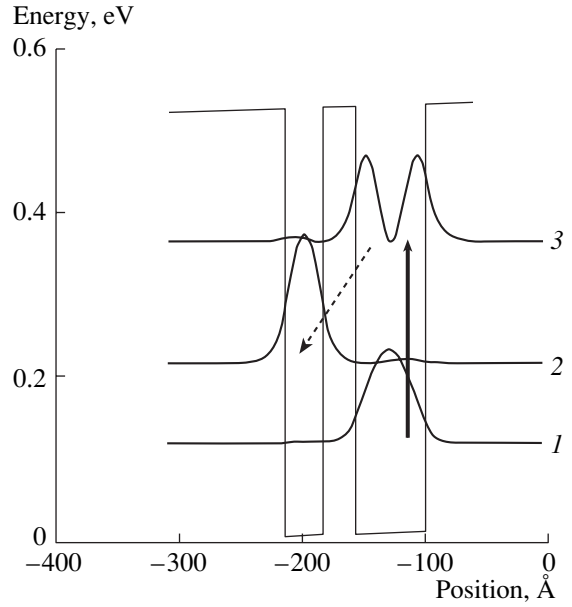

Fig. 3. One stage of the two-QW Raman active region in an InGaAs/AlInAs structure consisting of 3.2- and 5.8-nm QWs separated by a 2.5-nm barrier. The drive field (solid arrow) is nearly resonant to the transition *1–3* at 244 meV, while the Stokes field (dashed arrow) is generated at frequency $\omega_s = \omega_d - \omega_{21}$ and close to resonance with the transition *2–3*.

because the voltage across the compound active region remained essentially fixed by the laser threshold.

Tunability in conventional Raman lasers or amplifiers is associated with changing the wavelength of the external optical laser pump, while the amount of Stokes shift remains fixed and is determined by the phonon frequency. In the integrated devices, we have an opposite situation: the drive laser serving as an optical drive for the Raman laser is internally generated and its tunability is limited for the same reason as in standard QC lasers. However, the Raman shift is no longer fixed: It is determined by the energy separation between the subbands denoted by 1 and 2 in Fig. 3 below. If the transition 1–2 is diagonal in space, its energy can be efficiently tuned by the electric field (the linear Stark effect), if the voltage across the Raman region is independently controlled as in Figs. 1a, 1b.

The broadly tunable device with vertically integrated Raman and pump laser active regions is shown in Fig. 4. Note that the device is expected to generate the TM_1 modes that have a zero field at the position of a strongly doped side contact layer, thus, minimizing the losses. Also, the TM_1 mode provides a better confinement factor and the overlap of the drive field with the Raman region.

The Raman active region of the device in Fig. 4 can be an injectorless stack of coupled QWs. The absence of injectors increases the overlap factors of both modes with the Raman active region. The structure shown has large dipole elements z_{13} = 14 nm and z_{23} = 12 nm. Changing the electric field from 5 to 20 kV/cm shifts the Stokes frequency $\omega_s = \omega_d - \omega_{21}$ by as much as 12 meV from 148 to 160 meV, or by 100 cm^{-1}. The crucial question is whether this frequency tuning is accompanied by a large change in the Raman gain, which would affect the output intensity of the Stokes signal.

Obviously, this would be a very undesirable effect. The expression for the gain at the Stokes frequency that follows from the density matrix equations is shown below:

$$g_s = \frac{4\pi\omega_s e^2 z_{32}^2 \Gamma_s}{\hbar c \mu_s} \times \mathrm{Re}\left\{\frac{1}{\Gamma_{32} + |\Omega_d|^2/\Gamma_{21}^*}\left[\frac{|\Omega_d|^2 (n_1 - n_3)}{\Gamma_{21}^* \Gamma_{31}^*} - (n_2 - n_3)\right]\right\}, \quad (1)$$

where

$$\Gamma_{32} = \gamma_{32} + i(\omega_{32} - \omega_s),$$

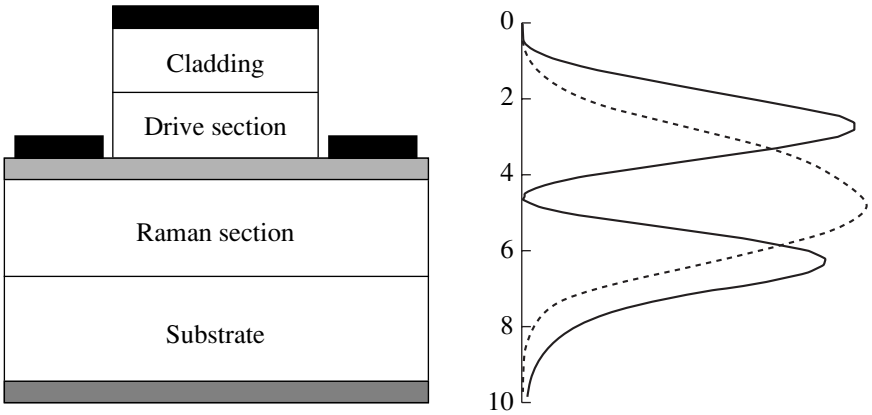

Fig. 4. Design of a broadly tunable Raman laser with independent biasing of the drive and Raman sections. Also shown are the magnetic field squared of the TM_1 mode (solid line) and TM_0 mode (dashed line) at the drive laser wavelength of 6 μm.

$$\Gamma_{31} = \gamma_{31} + i(\omega_{31} - \omega_d),$$

$$\Gamma_{21} = \gamma_{21} + i(\omega_{21} - \omega_d + \omega_s),$$

$\Omega_d = ez_{13}E_d/\hbar$ is the Rabi frequency of the drive mode, E_d is its electric field amplitude, z_{mn} is the dipole moment of the transition m–n, ω_d and ω_s are frequencies of the drive and the Stokes modes respectively, Γ_s is the optical confinement factor for the Stokes mode, and $\mu_s \sim 3.2$ is its refractive index. The optical drive field and the population densities $n_{1,2,3}$ of electrons in states 1, 2, and 3 are not free parameters. They must be calculated simultaneously from the same set of coupled density matrix and Maxwell equations. The only external parameters are the injection current and dephasing rates γ_{mn} for all transitions. The gain is maximized near the two-photon resonance $\omega_s = \omega_d - \omega_{21}$, where the generation of the Stokes mode is expected to occur. The ac Stark shift of the resonance given by the term $\sim|\Omega_d|^2/\gamma_{21}$ in the denominator of Eq. (1) is of the order of 2–3 meV for the intracavity drive power of the order of 100 mW.

We found that, with the same change in the electric field by 15 kV/cm that leads to a large shift in the Stokes frequency, the detunings of both drive and Stokes fields from their respective transitions 1–3 and 2–3 remain practically unchanged: their shift is only 1 meV. The dipole moments of these transitions are also changed very little—by less than 0.2 nm. The resulting change in the Raman gain calculated using Eq. (1) and neglecting any changes in the populations is only 3%. Therefore, the wide-range electric tuning of the Stokes radiation is not accompanied by a significant modulation of the output intensity. This is an important advantage of the device.

Next, we consider the possibility of Raman lasing in the devices with in-plane integration, such as that shown in Fig. 1b. First, we have to make sure that the active region for resonant Raman scattering can be created by simply applying a different bias to the QC laser active region. Interestingly, this seems to be the rule rather than the exception. Among the laser designs that we investigated, *all* QC laser active regions based on the vertical laser transition in coupled two or three QWs become Raman active regions at a near zero bias or at a small bias of the opposite sign. For example, in Fig. 5a, we show the QC laser structure reported by Gmachl et al. [17] at the electric field of 60 kV/cm. This corresponds to an above-threshold operation at photon energy 165 meV. In Fig. 5b, the same structure is shown at the bias of –10 kV/cm.

Clearly, laser photons can be used as a Raman pump detuned by about one or two FWHM from the transition 1–3 at 175 meV. Stokes emission is expected at the photon energy $E_{\text{Stokes}} = E_{\text{pump}} - E_{12} \sim 118$ meV, which is detuned from the transition 2–3 by the same amount ~10 meV. The dipole moments of the two transitions are $z_{13} = 10$ A and $z_{23} = 15$ A. These parameters are close to the optimal balance between resonant pump absorption and Raman gain. Furthermore, approximate resonance between the energy of laser pump photons and the intersubband transition energy E_{13} is maintained over a fairly large range of voltages applied across the nonlinear section. This happens because the transition 1–3 is vertical and experiences only the quadratic Stark effect. Meanwhile, the transition 1–2 is diagonal—its energy changes much more strongly with voltage. This paves the way for broadly tunable devices in the same way as was already discussed above.

3. FREQUENCY-UP CONVERSION

There is currently significant effort to push the wavelength of QC lasers into the short-wavelength mid-IR region below 4 μm. In the most mature and well-developed material system (InGaAs/AlInAs), the shortest attainable wavelength is limited by the band offset $\Delta E_c = 510$ meV. Moreover, the requirements of resonant tunneling and depopulation of the lower laser

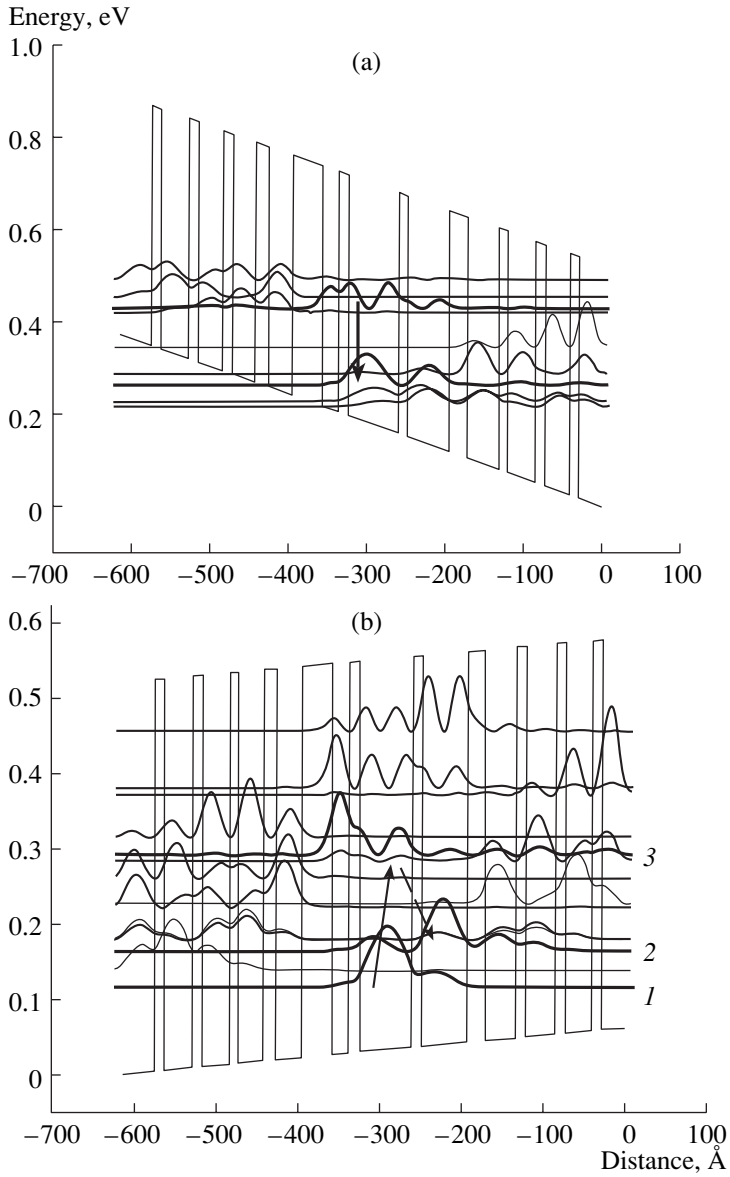

Fig. 5. (a) One stage of the three-QW active region of the QC laser reported in [17] at an electric field 60 kV/cm, corresponding to above-threshold operation at photon energy 165 meV. (b) The same structure at a –10 kV/cm bias serves as an intracavity pumped Raman active region. The drive field (solid arrow) is slightly detuned from the transition *1–3* at 175 meV, while the Stokes field (dashed arrow) is generated at photon energy $E_{\text{Stokes}} = E_{\text{pump}} - E_{12} = 118$ meV and close to resonance with the transition *2–3*.

level limit the energy of the laser transition to about 1/2 of ΔE_c, i.e., about 5 μm. In strained InGaAs/AlInAs structures, wavelengths of ~3.6 μm have been achieved. In heterostructures with a very large band offset, for example in the InGaAs/AlAsSb material system, one can have ΔE_c close to 2 eV at the Γ point. However, only a fraction of this band offset is actually available for lasing in QC devices pumped by resonant tunneling, because lateral L- and X-valleys are located only several hundred meV above the bottom of the conduction band of QWs in these materials. There are also growth and fabrication issues related to this material system.

We propose to generate short-wavelength radiation below 4 μm in our integrated nonlinear QC devices by frequency-up conversion of the intracavity optical laser pump via second harmonic generation (SHG) [2, 4, 6]. We have already demonstrated SHG at 5 μm wavelength with a milliwatt power level in InGaAs/AlInAs QC lasers operating at 10 μm [6]. However, 3-μm wavelength is unreachable in lasers of that design because of the need to accommodate both laser and the nonlinear cascade into the same QWs. In devices with a separately contacted nonlinear region, this becomes possible. Both in-plane and vertical integration strategies can be implemented. Figure 6 shows the double

QW region of a QC laser emitting at 6 μm that becomes the resonant SHG cascade at ~3 μm at the bias of the opposite sign. This design is suitable for in-plane integration.

Values of second order nonlinear susceptibility $\chi^{(2)}$ that can be achieved in the structures of the type shown in Fig. 6b are of the order 10^4 pm/V. They are mainly limited by the low dipole moment of the transition 1–3: $z_{13} \sim 0.2$ nm. Employing a vertically integrated design allows one to have complete flexibility in the SHG region design. As a result, much larger values of $\chi^{(2)} \sim 10^5$ pm/V can be achieved, of course, at the expense of a thicker structure and reduced modal overlap.

4. FREQUENCY-DOWN CONVERSION

Inversionless or Raman-type lasing could be especially valuable in situations when the population inversion is difficult to reach. One example of such a situation is lasing in the terahertz (THz) spectral region. With decreasing energy separation between subbands, it becomes increasingly difficult to provide selective injection to the upper laser state, selective depopulation of the lower state, and prevent backfilling of the lower state. These factors limit operation of existing THz QC lasers to cryogenic temperatures. The nonlinear optics may provide an alternative to usual lasing.

One possible Λ-type scheme for THz generation is shown in Fig. 7a. Here, the separation between states 2 and 3 is below the optical phonon energy. If these states are high enough above the ground state, their population is only due to the optical pumping. They are likely to have comparable lifetimes; therefore, the transition 2–3 has a population difference close to zero. The two-photon term in the gain expression in Eq. (1) is proportional to the population difference $n_1 - n_3$, which can be quite large if state 1 is the ground state or close to it. Therefore, potentially, the Stokes gain in the THz range can be much larger than the gain for standard lasing with inversion on the transition 2–3 and much larger than the gain in the mid-IR QC laser. Plugging the typical numbers into Eq. (1), we obtain the following scaling formula for the Raman gain:

$$g = \frac{\left(\frac{z_{32}}{5\ \text{nm}}\right)^2\left(\frac{n_{13}}{3\times 10^{16}\ \text{cm}^{-3}}\right)\left(\frac{\Gamma_s}{0.3}\right)}{\left(\frac{\lambda}{100\ \mu\text{m}}\right)\left(\frac{\gamma_{32}}{2\ \text{meV}}\right)}\left(\frac{1}{\gamma_{21}\tau_3}\right) 130\ \text{cm}^{-1}. \quad (2)$$

This estimate is obtained for the optimal value of the average drive intensity in the Raman active region $\frac{|\Omega_d|^2\tau_3}{\gamma_{31}} \sim 1$ corresponding to the drive power ~100 mW.

Of course, care should be taken to avoid too strong absorption of the drive on the transition 1–3, especially when this field is close to resonance. In particular, the dipole moment of the laser transition in the drive active region should be larger than z_{13} by at least a factor of 2.

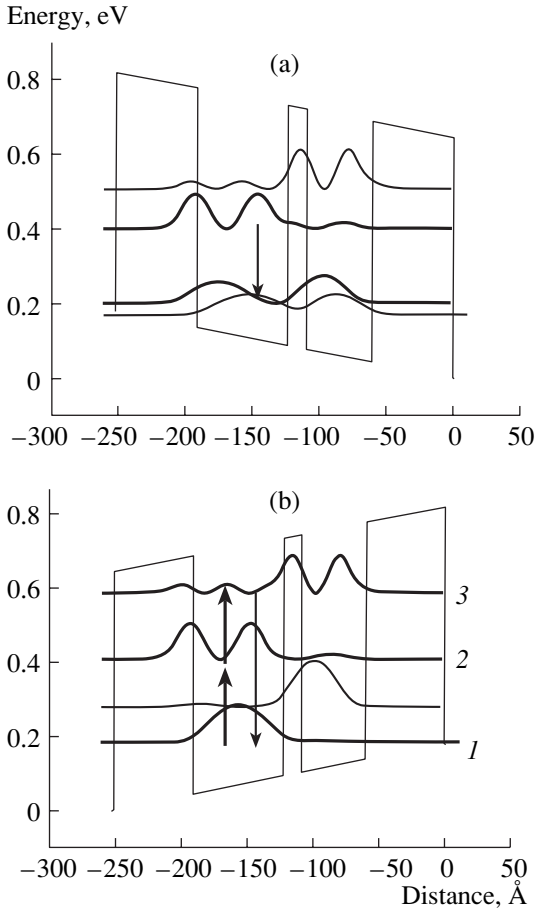

Fig. 6. (a) One stage of the two-QW active region of the strain-compensated $Ga_{0.41}In_{0.59}As/Al_{0.59}In_{0.44}As$ QC laser at a 6-μm wavelength and electric field 60 kV/cm. (b) The same structure at a –60 kV/cm bias serves as a resonant SHG cascade at a 3-μm wavelength with about 15 meV detuning of the pump field from the transition *1–2*, which is necessary to reduce resonant absorption. Relevant optical transitions are indicated by arrows.

The main challenge with the realization of the Raman or the optically pumped THz laser is a more complicated waveguide design. The waveguide needs to accommodate both mid-IR and THz modes and provide a good overlap between them. Probably, the simplest way to achieve this is to have a double metal or surface-plasmon THz waveguide and group the active region for the drive and Stokes fields in two separate stacks. Then, the whole Raman stack may be an injectorless doped multiple QW region or a superlattice, since we do not need any current injection to excited states (and, actually, no current at all) in order to obtain Raman–Stokes lasing. The Raman active region needs only optical pumping. An injectorless design saves space in the waveguide and helps to increase the optical

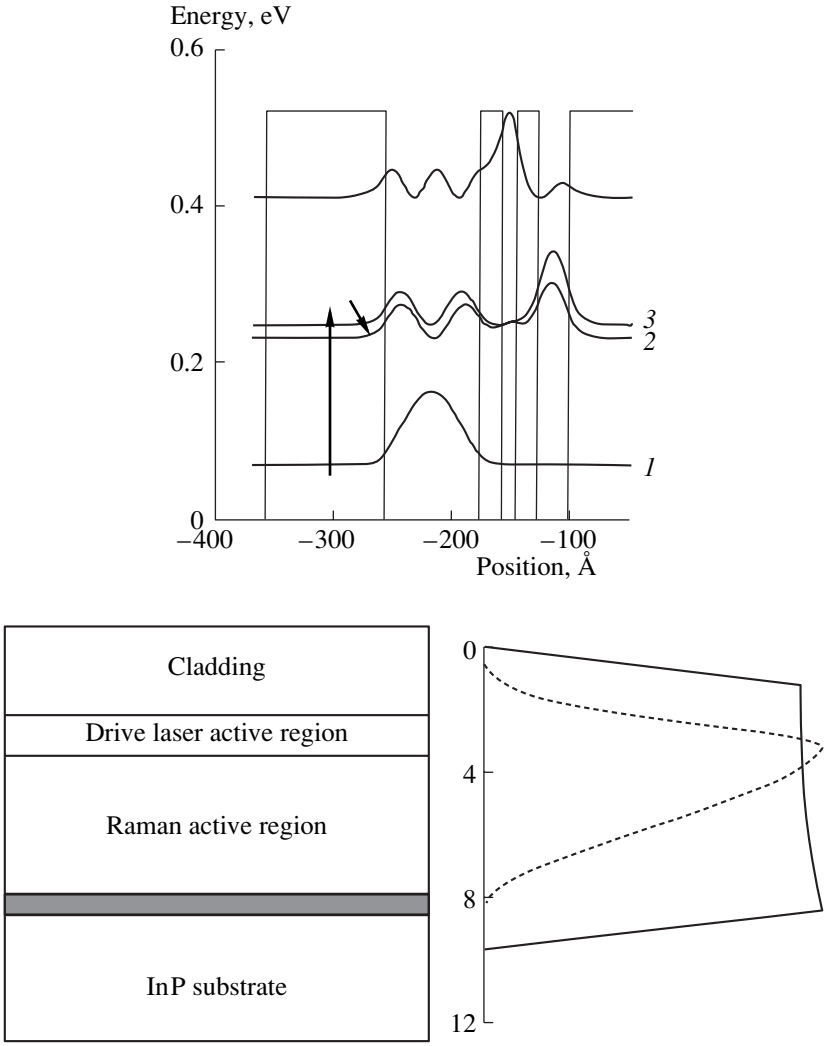

Fig. 7. (a) InGaAs/AlInAs three-QW structure for THz Raman lasing. (b) A sketch of the Raman THz laser with a double metal waveguide and separately stacked active regions for the drive and Stokes laser. Transverse profiles of the magnetic fields squared of the mid-IR drive ($\lambda_d = 7$ μm) and THz Stokes ($\lambda_s = 70$ μm) laser modes are shown with dashed and solid lines, respectively. Metal layers are shaded.

confinement factors. One example of such design is shown in Fig. 7b.

The THz losses are inevitably higher than in THz QC lasers, because both active regions must be doped in the range of 10^{16} cm^{-3} in order to provide high gain for both the drive and the Stokes fields. Typical numbers in the devices we modeled range between 40–100 cm^{-1}. These losses need to be compensated by a higher gain.

ACKNOWLEDGMENTS

This work was supported in part by NSF Grants ECS-0547019 (CAREER), EEC-0540832 (MIRTHE-ERC), ECS-0501537, and OISE 0530220, and AFOSR grants FA9550-05-1-0360 and FA9550-06-1-0338.

REFERENCES

1. N. Owschimikow, C. Gmachl, A. Belyanin, et al., Phys. Rev. Lett. **90**, 043902 (2003).
2. C. Gmachl, A. Belyanin, D. L. Sivco, et al., IEEE J. Quantum Electron. **39**, 1345 (2003).
3. C. Gmachl, N. Owschimikow, A. Belyanin, et al., Appl. Phys. Lett. **84**, 2751 (2004).
4. O. Malis, A. Belyanin, C. Gmachl, et al., Appl. Phys. Lett. **84**, 2721 (2004).
5. T. S. Mosely, A. Belyanin, C. Gmachl, et al., Opt. Express **12**, 2972 (2004).
6. O. Malis, A. Belyanin, D. L. Sivco, et al., Electron. Lett. **40**, 1586 (2004).
7. M. Troccoli, A. Belyanin, F. Capasso, et al., Nature **433**, 845 (2005).

8. A. Gomez-Iglesias, D. Wasserman, C. Gmachl, et al., Appl. Phys. Lett. **87**, 261113 (2005).
9. A. Belyanin, F. Capasso, and M. Troccoli, "Raman Injection and Inversionless Intersubband Lasers," in *Intersubband Transitions*, in *Quantum Structures*, Ed. by R. Paiella (McGraw-Hill, New York, 2006).
10. C. Gmachl, O. Malis, and A. Belyanin, "Optical Nonlinearities in Intersubband Transitions and Quantum Cascade Lasers," in *Intersubband Transitions in Quantum Structures*, Ed. by R. Paiella (McGraw-Hill, New York, 2006).
11. M. K. Gurnick and T. A. De Temple, IEEE J. Quantum Electron. **19**, 791 (1983).
12. M. M. Fejer, S. J. B. Yoo, R. L. Byer, et al., Phys. Rev. Lett. **62**, 1041 (1989).
13. C. Sirtori, F. Capasso, D. L. Sivco, et al., Appl. Phys. Lett. **59**, 2302 (1991).
14. F. Capasso, C. Sirtori, D. L. Sivco, et al., "Nonlinear Optics in Coupled-Quantum-Well Quasi-Molecules," in *Intersubband Transitions in Quantum Wells: Physics and Device Applications II*, Ed. by H. C. Liu and F. Capasso (Academic, San Diego, 2000).
15. G. Sun, J. Khurgin, L. Friedman, and R. A. Soref, J. Opt. Soc. Am. B **15**, 648 (1998).
16. H. C. Liu, I. W. Cheung, S. Thorpe, et al., Appl. Phys. Lett. **78**, 3580 (2001).
17. C. Gmachl, A. Tredicucci, F. Capasso, et al., Appl. Phys. Lett. **72**, 3130 (1998).